2-14-2008

Interactions between fMRI BOLD-activation during Reading Tasks and MRS-measured Metabolite Levels

Hassana Aisha Ibrahim
Yale University

Interactions between fMRI BOLD-activation during Reading Tasks and MRS-measured Metabolite Levels

A Thesis Submitted to the
Yale University School of Medicine
in Partial Fulfillment of the Requirements for the
Degree of Doctor of Medicine

by

Hassana Aisha Ibrahim

2007

ABSTRACT

INTERACTIONS BETWEEN FMRI BOLD-ACTIVATION DURING READING TASKS AND MRS-MEASURED METABOLITE LEVELS.

Hassana Aisha Ibrahim, Stephen Frost, Kenneth Pugh, Robert Fulbright. Section of Neuroradiology, Department of Radiology, Yale University School of Medicine, New Haven, CT.

Recent studies in the field of dyslexia have used magnetic resonance spectroscopy (MRS) to explore neurochemical manifestations of neurobiological differences in the brains of dyslexic adults compared to controls. This study examines the potential relationship between functional magnetic resonance imaging (fMRI) BOLD (blood oxygen level demand) activation scores in response to cognitive tasks and MRS-measured levels of a metabolite and a neurotransmitter, N-acetylaspartate (NAA) and gamma-aminobutyric acid (GABA) respectively, in the occipital region of brains of seven-year old children. Preliminary results from this multi-arm, longitudinal study indicate a significant positive correlation between fMRI BOLD signal elicited in response to picture-cues in the occipital region of interest bilaterally, and both GABA (R^2=0.477 p=0.05, 2-tailed) and NAA (R^2=0.587 p=0.01, 2-tailed) levels. The results suggest that the functional neuroanatomical circuitry involved in a cognitive task also has neurochemical indicators.

ACKNOWLEDGEMENTS

Alhamdullilah.

Thank you mom and dad for supporting me in my journey to becoming a physician.

Thank you Amina, Mohammed, Abdul, Ali for being such wonderful and fun siblings, and Hamza, for being a darling.

Dr Fulbright: thanks for being a mentor in every sense of the word. You were the best advisor I could have hoped for in writing this thesis.

Dr Pugh & Dr Frost: thank you for your invaluable help and time throughout this project.

Omar, Jessica, Leon, Raju, Courtney, Shobi, Nina: thanks for being wonderful friends to me in medical school.

I love you all!

TABLE OF CONTENTS

Content	**Page**
Introduction	1
Methods	20
Results	28
Discussion	31
References	39
Figures	45
Tables	51

INTRODUCTION

Background

Developmental dyslexia, the most common learning disability, is a disorder characterized by an impairment in reading abilities, which is not explained by deficits in intelligence, learning resources, socio-cultural opportunities or sensory acuity (1). Although there are several theories regarding its etiology, it is widely accepted as arising from a core deficit in phonologic processing (2, 3, 4). The neurobiological basis of the disorder has been explored through various approaches including from physiological, anatomical, genetic, and recently biochemical standpoints.

From a neurophysiological standpoint, using functional magnetic resonance imaging (fMRI), positron emission tomography (PET) and electrophysiology, studies have shown that compared to controls who show left planum temporale, perisylvian region (including the superior and medial temporal gyri) and left temporo-occipital activity lateralization in response to phonologic tasks (5), dyslexic children show a more diffuse response to such tasks (4, 6) and in some studies even a right hemispherical lateralization (7). In addition, Shaywitz et al. (8) found relative under activation in posterior regions (Wernicke's area, the angular gyrus, and striate cortex) and relative over activation in an anterior region (inferior frontal gyrus) in dyslexics compared to controls in response to phonologic tasks using fMRI. Paulesu et al. (9) found using PET a lack of concerted Broca’s and temporo-parietal cortical activation during phonologic tasks in dyslexics compared to controls, and also a complete lack of insula cortex activation. The findings led the Paulesu group to hypothesize a dysfunctional connection between anterior and posterior language regions in dyslexics.

Neuroanatomic findings in dyslexics using neuroimaging and post-mortem analysis have included reduced volume of the posterior language area (10), cerebellar anatomic differences (11), symmetry of the usually asymmetric planum temporale (although more recently challenged), dysgenesis and glial scarring of the inferior temporal gyrus (12)

As dyslexia tends to run in families, various candidate genes have been evaluated for heritability of the disorder (13, 14, 15). More than 30% of adults with developmental dyslexia report that at least one of their offspring manifested reading problems. Monozygotic twins also display almost twice the concordance in the diagnosis of developmental dyslexia than dizygotic twins (16).

Although relatively fewer studies have been conducted to explore biochemical differences between dyslexics and controls, nonetheless, these studies have found various dissimilarities in metabolites and neurotransmitters. Using magnetic resonance spectroscopy (MRS), Rae and others (17) found significant differences between dyslexic men and controls in ratios of choline-containing compounds (Cho) to N-acetylaspartate-containing compounds (NAA) ($p<0.01$) in the left-temporo-parietal lobe and Cho to creatinine-containing compounds (Cr) in the cerebellum. Specifically, there was a decreased Cho/NAA ratio in the left temporo-parietal lobe, no difference in Cr/NAA ratio, and also a decreased Cho/Cr ratio (non-significant) in dyslexic men compared to controls, suggesting that the decrease in the Cho/NAA ratio was from a decrease in Cho. There was also a significant and relatively lower Cho/NAA ratio in the left temporo-parietal lobe of dyslexics compared to the right ($p<0{\cdot}02$), which was lacking in controls. As hypothesized by previous authors concerning neuroanatomical differences (12), the

Rae et al group also suggests that the observed neurobiochemical differences reflect changes in cell density. They further hypothesize that it is a result of abnormal development of cells or intracellular connections or both.

A study by Richardson et al., using ^{31}P-MRS in 1997 (18), found significant elevation in phosphomonoester (PME) peak area in dyslexics; consistent with a hypothesis that membrane phospholipid metabolism is abnormal in dyslexia. The PME peak predominantly consists of phosphoethanolamine (PE) and phosphocholine (PC), which are precursors of membrane phospholipids. And in 1999, Richards et al. (19), found that dyslexic children differ from controls in brain lactate metabolism when performing language tasks, but not in non-language auditory tasks. Other studies by Richards et al. (20) have examined changes in metabolite levels following behavioral interventions in children with dyslexia. Their group found that prior to therapeutic intervention, the dyslexic group showed a significantly greater increase in lactate levels in the left frontal regions (including inferior frontal gyrus) during phonologic tasks. After treatment, the dyslexic group did not differ significantly from the control group in lactate levels in any brain region during tasks, but found that the treatment effect was due to the morphologic component of the tasks, rather than the phonologic component.

The importance of metabolite differences lies in their use as a tool reflective of different brain cells and/or structures. For example, the concentration of Cho is higher in white matter than in grey matter, and higher in glial cells than in neurons, whereas NAA occurs primarily in neuronal cells and is a marker of neuronal-cell density and neuronal-mitochondrial activity in the brain. These correlations have been confirmed by histochemical and cell-culture studies (17). NAA has been associated with lower IQ in

such disorders as mental retardation and temporal lobe epilepsy. White matter NAA has also been related to broad measures of cognition in normal young and elderly subjects, implicating NAA as a sensitive marker of brain–behavior relationships (21).

In addition to metabolites, neurochemicals that function as neurotransmitters are also important potential candidates for understanding the biochemical manifestations of neurobiological disorders. GABA is an inhibitory neurotransmitter that has been previously linked to epileptic seizures, among other neurological diseases. In the context of reading disabilities, various GABA-modulating drugs have been shown to affect performance in learning tasks in rodents (21, 22). There is also growing evidence supporting a hypothesis that the GABAergic (and cholinergic) system plays a key role in neuronal plasticity necessary for repetition adaptivity (24). Coupled with the fact that a number of GABA gene mutations have been found in the susceptibility region for dyslexia (25; 26), GABA appears to be a suitable neurotransmitter candidate for reading disabilities. In a recent study by McLean et al. (27), the authors successfully measured in vivo levels of GABA using MRS and established a control range of GABA levels in the occipital lobes of volunteer participants.

As discussed above, a number of interrelated neural systems have been proposed as key in reading ability. One such system has been proposed in the left occipital-temporal region. It is hypothesized as a rapidly processing reading system that is important for the development of skilled reading, functioning as an automatic, instant word-recognition system. In addition, brain activation in this region increases as reading skill increases (28). The MRS arm of this study focuses on an occipital region as the region of interest for the MRS voxel. Ideally, the MRS voxel would be placed in both left

and right regions for comparison, however, for practical purposes, the ROI will be chosen in a central location, described further in the methods section.

The information gathered from using a non-invasive modality such as MRS is important not only to better understand the neurobiology, but also as a platform to design and monitor therapeutic interventions. Also importantly, majority of studies on reading disability have been conducted using adult dyslexics, and the relative safety and non-invasiveness of MRS and fMRI permits easier recruitment of pediatric subjects for studies, improving the ability to establish the neurobiological etiology of dyslexia, and increases the possibility of earlier intervention.

STATEMENT OF PURPOSE AND HYPOTHESIS

The study is part of a multi-dimensional, longitudinal project (by the Yale University School of Medicine Neuroradiology section of the Department of Radiology, Yale Reading Center and Haskins Laboratories) using MRS, fMRI, genetic and behavioral analysis to examine reading disability. The preliminary result presented in this thesis explores interactions between both NAA and GABA levels in the occipital region of interest as measured using MRS, and fMRI BOLD activation scores in response to picture processing.

We hypothesize a correlation between MRS-measures of GABA, NAA and BOLD activation scores and also between GABA and NAA levels, and that these values will affect reading performances over time.

Introduction to MR

Before presenting and discussing the results of this study, the basis of magnetic resonance will be reviewed to better understand the data and also the strengths and limitations of clinical MRS and fMRI.

Without doubt, the concept of magnetic resonance (MR) has revolutionized medical diagnosis. This is more commonly thought of as magnetic resonance imaging (MRI), however, nuclear magnetic resonance spectroscopy (NMR) or magnetic resonance spectroscopy (MRS) is another application that is increasingly being appreciated and applied in diagnostic medicine. The concept of MR has been applied in basic science laboratories for decades to identify chemical compounds and analyze molecular interactions, however it was only first used for imaging humans in the 1970s. And by the late 1980s, MRI had become the popular modality for assessing neurological disorders and evaluating vascular flow (29). In addition to its employment in identifying compounds and defining structures, one of the greatest appeals of MR modality in medicine lies in its use of non-ionizing radiation, thereby avoiding the more destructive nature of comparable imaging modalities such as computed tomography (CT).

Both MRS and MRI essentially employ similar principles of MR. Whereas MRI uses the signal obtained to generate an image; MRS generates a frequency domain spectrum of the components of the object (30). From the image generated in MRI, structural anomalies can be detected, providing useful information about diseases. MRS on the other hand provides biochemical information about pathology and may lend a better understanding of underlying pathological processes. Unlike MRI, which primarily observes hydrogen nuclei to obtain information about water and fat constituents of tissue,

MRS provides information on the nature and concentration of non-water protons present in metabolites and chemicals present in tissues. Although ^{1}H is highly abundant in organic compounds, the ^{1}H MR spectral range is very narrow and signal obtained usually contains undesired noise signals from other molecules. However, MRS can also interrogate other nuclei such as ^{13}C, ^{15}N, ^{19}F and ^{31}P (31). These nuclei are also important components of organic compounds. For instance, nitrogen is found in proteins and deoxyribonucleic acid (DNA), and carbon is a crucial component of organic compounds. However, signals from such nuclei are usually obtained from molecules with much less concentration than water in tissues, and consequently one of the limitations of MRS is that spectra have to be acquired from relatively large volumes of tissue ($>1cm^3$) compared to MRI.

fMRI is a newer brain mapping technique that was first used in human experiments in the early 1990s. It is based on MR and uses rapid imaging techniques to demonstrate regional blood flow changes in space and time in response to performance of various sensorimotor and cognitive tasks. The fMRI phenomenon is actually dependent on tissue fluctuations of paramagnetic deoxyhemoglobin and diamagnetic oxyhemoglobin, which causes changes in magnetic susceptibility. It is assumed that blood flow changes provide an indirect measure of brain activity based on neurovascular coupling, i.e. increased blood flow in response to increased neural activity. fMRI provides excellent spatial resolution, enabling matching of blood flow changes to specific anatomic structures (29). The differences in MR signal intensity between two conditions are typically presented as a color scale, representing statistical significance, either

displayed over the original images or superimposed over a high-resolution anatomic image (32)

Recent improvements in hardware and measurement techniques have also contributed in making in vivo clinical MR studies practical by providing an acceptable signal/noise (S/N) ratio without unbearably prolonging patient time in the scanner, and also streamlining processing of data.

Basic science of MR

Magnetic resonance probes atoms and molecules based on their interaction with an external magnetic field (31). It primarily relies on one of the characteristics of an atom – its nuclear spin. To review, an atom is composed of protons and neutrons (which make up the core nucleus) and electrons (which surround the nucleus). All atoms of an element have the same atomic number, i.e. the same number of protons in the nucleus. They can however differ in the atomic weight and are referred to as isotopes. The difference in weight is essentially due to differences in number of neutrons, as electrons contribute relatively little to atomic weight. This elemental characteristic is also important because the relative abundance of various isotopes affects the way the nucleus of an element can be examined using MRS.

As mentioned above, the intrinsic motion of an atom - its nuclear spin is necessary for the concept of magnetic resonance. This spin can be described using quantum mechanics or classical mechanics. Classical mechanics assumes that a moving object being studied is a point particle, with negligible size, and its motion can be described by its position, mass and external force being applied to it. This often suffices when describing larger size objects e.g. atomic level and larger, but becomes inaccurate

when examining objects at sub-atomic levels. Quantum mechanics is a modern mathematical theory, which provides a more complete, accurate and precise description of elemental properties on atomic and sub-atomic levels, albeit more complex as compared to classical mechanics. The term quantum refers to the assumption that certain physical properties can only assume discrete quantities, as in the case of nuclear spins.

The quantum mechanics theory states that the discrete and quantized nuclear spin value is either zero (i.e. no spin), integer (e.g. 1, 2, etc) or half-integer (e.g. 1/2, 3/2, etc). A zero spin value is a result of an atom having an even number of protons and neutrons e.g. ^{12}C, and as such cannot be studied using MR. An integer value is found in an atom with an odd number of protons and neutrons e.g. ^{2}H, while a half-integer value is found in an atom with an even number of protons and odd number of neutrons or vice versa e.g. ^{1}H. The half-integer spin value is the most commonly encountered in clinical spectroscopy, but both whole and half-integer values provide a nucleus a magnetic field. This magnetic field can be likened to a bar magnet with a magnitude (i.e. integer or half-integer) and orientation (i.e. north and south poles). The nuclear magnetic field can be measured to obtain information about that molecule and its surroundings. This is done indirectly by manipulating the nuclear spin with a radiofrequency (RF) pulse, and measuring the resulting voltage.

To further explore why the radiofrequency pulse manipulation is necessary, consider a volume of tissue outside a magnetic field containing various nuclei, but all having a nuclear spin magnitude of 1/2. Although each nucleus behaves like a tiny magnet, the net magnetization of the tissue is zero. This is because the nuclear magnetization effectively cancel each other out because they are oriented randomly i.e.

$_{+}{}^{1}/_{2}n + {}^{-1}/_{2}n = 0$ (where n = number of nuclei in that orientation). If the same tissue is placed in a magnetic field, B_o, of a given magnitude and axis of orientation, the individual nuclei spins will start to rotate parallel to the axis of orientation of the external magnetic field. They will however be slightly tilted away (precess) from the axis of the magnetic field because of the continuous interaction between the moving nuclear spins and the external magnetic field. An analogy of precession is the wobbling of toy tops as they spin.

Each nuclear spin has a z-axis component, which is parallel to that of the external magnetic field B_o, and constant with time, and x- and y-axis components referring to its precession, which is constantly changing and perpendicular to the external magnetic field (31). The Larmor equation relates the strength of the magnetic field B_o to the rate of precession as follows:

$$\omega_o = \gamma B_o / 2\pi$$

Where, ω_o = Larmor frequency in Megahertz (MHz), B_o is the magnetic field strength that the spin experiences in tesla (T) and γ is the gyromagnetic ratio, a constant for each nucleus in units of reciprocal seconds, reciprocal tesla ($s^{-1}T^{-1}$).

When an external magnetic field is applied on a magnetic dipole, in this case the "nuclear magnet", it will exert a rotational force (torque) and result in magnetic potential energy. The Zeeman interaction defines the possible values of the resultant energy states of the nuclear spin, in the *z*-axis. For a given magnitude of spin, I, the possible values of the *z* component is equal to 2I + 1, symmetrically divided about 0. In addition, the difference in *z* component values between adjacent orientations is equal to +1 or –1 (31). Therefore, for example a spin magnitude of 1/2 has only two possible values of the z

component, +1/2 and –1/2, also known as spin up (parallel) and spin down (antiparallel) respectively. A similar interaction occurs for energy levels, where for most nuclei, the lowest energy state is at the largest positive z component (i.e. parallel to B_o) and the highest possible energy state corresponds to the largest negative z component (i.e. antiparallel to B_o). The difference in energy level between each consecutive state is proportional to B_o, and the corresponding frequency is the Larmor frequency of the spin. And if energy is applied to the nucleus at the Larmor frequency (also known as the resonant frequency), the spin will go from one energy level to another through a process known as resonance absorption.

As the spins examined in clinical MRS are usually from a bulk of tissue, rather than individual nuclei, the Boltzmann distribution is useful in describing the energy states of a collection of spins:

$$N_i = N_{total}\, e\, (-E_i/kT)$$

Where N_i is the number of spins in state I, which has energy, E_i in Joules (J), N_{total} is the total number of spins in the volume, k is the Boltzmann's constant (1.381×10^{-23} J K^{-1}) and T is the absolute temperature in Kelvin (K). This relationship indicates that the largest number of spins will be in the lower energy states with gradually reduced numbers in higher energy states.

If an RF pulse is applied to a collection of spins, majority of spins (those in a lower energy state) will absorb energy, while a minority (those is a higher energy state) will emit energy. The RF pulse is applied at a frequency ω_1 (central frequency) and oriented at a magnetic field of B_1 (which is perpendicular to B_o). If the RF pulse is applied at the Larmor frequency (ω_o), the net magnetization of the tissue (M_o) will rotate

away from its equilibrium orientation towards the transverse plane. And if applied long enough at the right amplitude, M_o will rotate completely to the transverse plane. This transverse plane is perpendicular to both B_o and B_1, and such an RF pulse is known as a 90^o pulse.

When the RF pulse is discontinued, the spins will return to their original orientation and energy state, and will emit energy at the Larmor frequency, ω_o, in the process. During this precession, a voltage is emitted in the transverse place, and can be measured by a loop of wire in that plane. The magnitude of the voltage is dependent on the value of M_o immediately prior to the 90^o pulse and it will decay with time through a process known as relaxation. This voltage is the MR signal, and is known as free induction decay (FID).

It is important to remember that in a tissue sample, each individual spin will experience its own magnetic field; hence several voltages (MR signals) at different frequencies will be obtained following an RF pulse. Therefore, the FID of a tissue sample actually contains many superimposed frequencies as a function of time. In order to separate the individual frequencies, the amplitude of the voltage can be expressed as a function of frequency, rather than time (FID). This is done via a mathematical process called Fourier transformation.

In addition, each voltage wave can be defined in terms of phase, i.e. its frame of reference or position in the cycle, along the time domain. Most MR receivers examine two phases; one with the reference signal in phase with the original transmitter, and the other 90^o shifted in phase. These signals are called the real (dispersion) and imaginary (absorption) channels respectively. The Fourier transformation actually produces spectra

containing a mixture of these two phases/modes; therefore, a process known as phase correction is employed. This enables further analysis to be performed on each spectrum, more commonly the absorption spectrum.

So how does one interpret the spectrum? There are three characteristics of the spectrum that are of utmost interest: the integrated area, position (resonant frequency), and width of each resonance peak. The peak area is proportional to the number of spins contributing to the MR signal. The x-axis peak position has information about the type of spin and its molecular environment, reflecting the degree of "chemical shift" of the molecule. This is usually time independent, but can also vary with time. The third characteristic of interest, the width, conveys information about whether the signal is from one type of spin, or multiple types. This is most accurately performed by determining the shape of the spectral peak. Most tissue MR spectra are composed of two types of line spectra shape, Lorentzian and Gaussian. Lorentzian shapes have very broad bases, and are such that the line width [half-width at half-maximum height (hwhm)] is inversely proportional to the total transverse relaxation time, T2*. These are usually from spins in a single molecular environment. Gaussian line shapes on the other hand, are observed when multiple spins with very similar environments contribute to the resonance.

Time-independent MR modifiers: chemical shift, spin coupling

Thus far, the nuclear magnetic field has been described by its relationship to an applied magnetic field of known magnitude. However, the total magnetic field experienced by a nucleus is modified by the currents induced by electrons present in orbits around the nucleus, a concept referred to as chemical shift. As such, there can be variations in NMR frequencies of the same type of nucleus, due to differences in electron

distribution in different molecules e.g. from different bond lengths, bond angles, binding patterns. Chemical shift is usually expressed in parts per million (ppm), and is calculated from the difference in precession frequency between two nuclei (hertz) divided by the Larmor frequency of the magnet (Megahertz). The size of the chemical shift is given with respect to a reference frequency, usually a molecule with a barely distorted electron distribution, such as tetramethylsilane (TMS). For example, lactate (methyl group) has a chemical shift of 1.3 ppm, 2.0 ppm for NAA (methyl group) and 4.7 ppm for water, all relative to TMS.

Another important time-independent modifier in magnetic resonance frequency is spin coupling. This refers to the sub-division of a peak from a single proton into multiple peaks on the NMR spectrum as a result of interaction with nearby nucleic spins within a molecule. This splitting of NMR lines conveys more detailed information about the structure of molecules. Spin-spin coupling or *J* coupling is a sub-type of spin coupling, which denotes facilitation by nearby electrons. Spin-spin coupling is different from chemical shift, because the former is independent of magnetic field strength and always involves another spin, while the latter is altered by magnetic field strength. The number of multiple peaks (multiplets) arising from a proton is proportional to the number of similar protons connected by double or triple bonds to the proton being observed (31).

Time-dependent MR modifiers: relaxation, spin echo

Relaxation and spin echo are two examples of important time-dependent interactions in MR. As described earlier, nuclei with spins in lower energy states absorb energy or become “excited” when an RF pulse is applied. Relaxation describes the release of the absorbed energy and return of the nuclei to their original states. This

energy release can be measured in longitudinal and transverse directions, involving T1 and T2 time constants respectively. T1 relaxation time is the time required for the *z* (longitudinal) component of the magnetic field (M_0) to return to 63% of its original energy value following excitation, and it follows an exponential curve. T1 is also known as spin-lattice relaxation time because this relaxation generally occurs by interactions between the nuclei of interest and their environment or "lattice," consisting of unexcited nuclei and electric fields in the surroundings. Transfer of energy from excited nuclei to the lattice is facilitated by having unexcited nuclei with similar intrinsic frequency to that of the resonant frequency. There is less discrepancy in these frequencies when macromolecules such as proteins with slower tumbling rates (lower frequencies) are considered, than in smaller molecules with faster tumbling rates such as metabolites. Hence protein nuclei generally have shorter T1 values than metabolites. At a field strength of 1.5 Tesla (T), lactate (methyl group) and NAA (methyl group) metabolites from brain occipital lobe have T1 values of 1.55s and 1.45s respectively (31).

T2 relaxation time is the time required for the transverse component of the magnetic field (M_0) to return to 37% of its initial value following excitation, via irreversible processes. As this is perpendicular to the ambient magnetic field, the decay occurs mainly due to interactions between the nuclei of interest and other excited nuclei. Hence T2 is also known as spin-spin relaxation. Immediately following a 90^o RF pulse, spins will absorb energy, orient in the transverse plane, align in the same phase and precess at the same frequency. This precession at the same frequency and phase facilitates energy transfer between adjacent nuclei, rather than to their environment (as in T1). However, an irreversible loss of transverse magnetization signal eventually occurs

because of local microscopic field inhomogeneities. An example is the fluctuation as a function of time of the local fields produced by electrons of molecules in motion relative to the spin of interest (33). At a field strength of 1.5 tesla (T), lactate (methyl group) has a T2 value of 1040ms.

T2 does not take into account the intra-voxel dephasing that occurs due to macroscopic field inhomogeneities. This dephasing results in a much faster decrease in transverse magnetization, T2*, via free induction decay than predicted by T2. T2* like T2, measures the time it takes for the transverse magnetization to decay to almost zero, but takes into account the faster decay resulting from dephasing. As such, T2* is often referred to as the true "relaxation" time and is always less (shorter) than the T2 relaxation time. Both T2* and T1 are also greatly influenced by variations of field strength, unlike T2 (33).

Sequences that accentuate T1 decay are generally referred to as T1-weighted images and those that accentuate T2 relaxation are referred to as T2-weighted images. A combination of these is usually employed in brain MR scans, as some abnormalities may be better displayed on one versus the other. Fluid such as cerebrospinal fluid is generally very bright on T2-weighted images and dark on T1-weighted scans. Whereas fat is bright on T1-weighted images and dark on T2-weighted images. The intensity of brain tissue is somewhere in the middle, and the intensity of blood vessels varies depending on velocity of blood flow (29).

Spin echo refers to a maximal MR signal obtained when all the spins in a volume of interest have the same phase. This is obtained by applying a second rf pulse at 180^{o} at a later time, following the initial 90^{o} rf pulse, resulting in refocusing or rephasing of the

spins. A common analogy is by considering two runners A and B, who begin running at time zero from the same starting point in the same direction along the y-axis, at speeds of 10 miles/hour and 20 miles/hour respectively. If both runners are stopped after an hour, A will be at +10 miles and B will be at +20 miles along the y-axis. However, if they are both allowed to run back toward the original starting point at previous respective speed along the y-axis, after an hour, both runners A and B will be back at the starting point. This illustrates that regardless of the local field inhomogenities that cause spins to precess at different rates, the spins are refocused following the 180^{o} pulse**.** Gradient echo unlike spin echo is obtained through application of a specifically calculated excitation pulse that removes necessitation of a rephasing rf pulse. There are differences in quality and contrast of images obtained using different approaches (34).

Localization techniques: STEAM, PRESS

Stimulated echo acquisition mode (STEAM) and point-resolved spectroscopy (PRESS) are two single-volume localization techniques employed in MRS. STEAM sequence is a form of spin echo which uses an initial excitation rf pulse (classically 90°, but could be anything other than 180^{o}), followed by two rf pulses (classically 90°, 90°), producing the stimulated echo after a time delay (equal to the interval between the first two pulses) following the 3^{rd} pulse. The intensity of the resultant echo is partly dependent on the T1 relaxation time because the excitation is 'stored' as longitudinal magnetization. PRESS uses a 90° rf pulse, followed by two 180^{o} pulses. The 90° rf pulse rotates the spins in the yx-plane, followed by a 180° pulse in the xz-plane and another 180° pulse in the xy-plane, producing the echo. STEAM uses a shorter TE, has better suppression of water, and thus allows for visualization of more metabolites including

myoinositol, glutamate, glutamine, and GABA. PRESS on the other hand uses a longer TE and results in loss of signal from most brain chemicals except NAA, creatinine, choline-containing phospholipids, and lactate; however, it is not as susceptible to motion, diffusion, and quantum effects and has a better signal to noise ratio than STEAM.

Reduction of external magnetic field inhomogeneities: shimming

Shimming is a technique of correcting the inhomogeneities of the external magnetic field caused by intrinsic imperfections of the primary magnet or from other ferromagnetic objects present in the surroundings. It is done most commonly by using shim coils and making changes to their currents while obtaining the Fourier transform signal.

Clinical applications of MRS, fMRI

Currently, MRS (specifically ^{1}H) of the brain is the most commonly performed MRS patient examination. The brain is an ideal target organ for MRS compared to other organs because of more favorable characteristics, such as less motion artifact, relative ease of shimming**,** and lack of detectable (i.e. mobile) lipids in normal brain tissue. (31).

Brain MRS studies have focused on metabolites such as N-acetyl aspartate (NAA), which is a neuronal marker; choline, an indicator of cell membrane turnover; creatine, a marker for energy metabolism; and lactate, a marker for anaerobic metabolism. Clinical CNS applications of MRS have included evaluations of tumors post-surgical resection to assess for residual or recurrent cancerous tissue (29). It is mostly used as an adjunct to MRI. ^{1}H MRS has also been used to monitor treatment in patients undergoing chemotherapy for leukemia, by examining lumbar vertebral body bone marrow fat. Some studies have suggested future applications of MRS in assessment

of muscle disease by comparing signals from fat peaks and relative water/fat concentration (31).

Clinical applications of fMRI have included presurgical mapping of important eloquent brain regions, to guide decision of candidacy for surgical resection of adjacent abnormal tissues such as tumors or epileptic foci (29). Future clinical fMRI applications are anticipated in the diagnosis and monitoring of probable Alzheimer's disease, learning disabilities and other neurological disorders.

MATERIALS AND METHODS

Subjects

The subjects included in this analysis are the initial recruits of a longitudinal study to examine the neural circuitry for reading from the beginnings of instruction to more advanced skill levels (ages 7.5-10.5) in non-impaired (NI) and reading disabled (RD) children. Eighteen children were recruited prospectively over a 6-month period. The subjects were 8 boys (mean age at fMRI testing = 8 years and 2 months; SD = 6 months; range from 6 years, 9months to 10 years, 3 months) and 10 girls (mean age at fMRI testing = 7 years and 10 months; SD = 1 year; range from 7 years to 8 years, 9 months). The definition of reading disability (RD) is based on the Wechsler Intelligence Scale for Children-III (35) Full Scale IQ and the Decoding (Basic Reading cluster) score from the Woodcock-Johnson Psychoeducational Test Battery-Revised (36). To participate in the study, all children had a Full Scale IQ of 75 or above on the WISC-III. Children will be defined as RD on the basis of a score below the 21st percentile on the Basic Reading cluster of the Woodcock-Johnson. This definition specifically excludes children who have reading scores that are discrepant with IQ, but who have reading scores above achievement cutoff (22nd percentile and higher). Decoding definitions are used because of evidence that these measures most reliably and validly define the largest group of children with RD (37, 38, 39). Each child was evaluated behaviorally, with MR spectroscopy, and with fMRI, at the time of recruitment. The MRS and fMRI studies were performed on different days, not more than 2 months apart from each other.

^{1}H Magnetic Resonance Spectroscopy

MRS was performed with a 4-Tesla magnet with a 94-cm bore and a Bruker Avance spectrometer. GABA was detected using a spin-echo J-editing measurement (40).

A surface coil was placed against the back of the head. For voxel positioning, gradient-echo scout images with a nominal axial orientation were acquired from slices 1.5 mm thick, with no slice gap and a field of view of 200 mm, divided into 128x128 pixels. For each measurement, the water signal was used to calibrate the pulse power for the spin-echo sequences and the selective inversion pulse used for the J-editing of GABA.

The GABA-editing sequence was run in blocks of 22 minutes, yielding 27 twenty-second pairs of sub-spectra that were subtracted to obtain the edited GABA signal. Briefly, one sub-spectrum was acquired with an inversion pulse applied to the GABA C4 proton, and one sub-spectrum was acquired without the inversion pulse. The phase of the coupled GABA C4 proton resonance was inverted in one sub-spectrum relative to the other, but the other, uncoupled, resonances in the region (e.g., creatine and choline) were the same in both spectra. When the two-spectra were subtracted, creatine and choline vanish, leaving the GABA. The data were acquired in interleaved fashion, toggling between individual inverted and uninverted acquisitions in 20-second blocks. Each block was stored and the sequence was run for 22 minutes to yield 27 pairs of sub-spectra. Sub-spectra were acquired with 1024 data points in a 410-ms acquisition, a 3-second repetition time, and a TE of 68 ms.

To adjust for cortical atrophy, it is necessary to quantify the content of GM, WM, and CSF in the MRS voxel that was used for GABA detection. The T_1 relaxation rate of

gray matter, white matter, and CSF differ significantly, with values of 787 ± 47, 1236 ± 69, and 3320 ± 325 ms at 4T (n=6, mean ± SD). Therefore, T_1 can be used to discriminate among the different tissue types in the brain, through image segmentation by tissue type. To permit image segmentation, quantitative images of T_1 were obtained using an inversion-recovery measurement with the surface coil in the same experimental session. However, the surface coil has very inhomogeneous B_1 that must be measured in addition to the inversion-recovery images.

A B_1 map (Figure 1) consisting of 7 contiguous 3-mm slices were acquired perpendicular to the short axis of the voxel, to span the 1.5-to-2 cm thickness of the occipital or frontal GABA voxels, or 14 3-mm slices to span the 4-cm thickness of the ^{13}C voxel. For the GABA voxel, the 4 slices more distant from the coil were acquired using 3 dB less power than what is used for the 3 slices closest to the coil. The different pulse powers were selected to yield a nominal flip angle of 40°-50° for each of the slices, whether near or far from the coil. The sequence works by the acquisition of two gradient echo images obtained with pairs of sinc pulse excitations separated by 20-30 ms. The ratio of the images yields an image of the cosine of the individual excitation angles. Given the sinc pulse parameters of the amplitude, time, and shape, an image of the B1 (Hz) was determined from the image of the excitation angle. Because B1 varies slowly across space, the two sets of images were acquired with a 240-mm field of view and 64 x 64 resolution, with a total acquisition time of 1.5 min.

An inversion-recovery MRI was acquired with 3-mm slices to span the MRS voxels. For GABA, 7 contiguous slices were acquired, with a 240 mm field of view and 256 x 256 resolution, spanning the 1.5-cm voxel thickness, using rapid inversion-

recovery sampling method (41) optimized statistically for sensitivity (42). Briefly, a single global inversion pulse was applied using a 3-lobe hyperbolic secant pulse (43) and gradient echo acquisitions of individual lines of k-space were acquired over two seconds following the inversion to sample the inversion recovery curve of the tissue water. Due to overlap of slice excitation profiles, it is necessary to acquire half the slices in one set and the other half of the slices in another set. For example, the 7-slice image set consists of two sets of excitations (slices 1, 3, 5, 7, and slices 2, 4, 6). The total acquisition time for the quantitative T1 imaging and segmentation was 8 min for GABA.

The paired images were processed using software written in MATLAB. After Fourier-transformation, the first image of each pair was phased so that each pixel is purely real, and the identical phase was applied to the second image of each pair. Basing the phasing of the second image on that of the first permits the identification of flip angles whose cosine is negative. The ratio of the second image to the first yields an image of the cosine of the effective pulse angle in each image pixel of each slice, and the arc cosine of the image provides the effective pulse angle. The effective pulse angle was converted to effective B1 based on a product-operator simulation of the frequency dependence of the pulse angle across the slice, thereby creating an image of B1 for each slice across the MRS voxel.

After Fourier-transformation, the images were phased and, pixel-by-pixel, fitted with a simulation of the IR pulse sequence, using the B_1 measured in the B_1 maps. The result of the fitting is a multi-slices set of quantitative images of T1. The quantitative images of T1 were converted to images of percent GM, WM, and CSF (44), called graded segmented images. From the segmented images and the known dimension and position

of the MRS voxel used for GABA detection, the composition of the MRS voxel was determined as percentages of GM, WM, and CSF based on an empirical calibration curve of mixtures of GM, WM, and CSF. Figure 2 is an example of this procedure.

Spectral Analysis

Using software written in MATLAB (the Mathworks, Inc.), each sub-FID was phase-locked using the water FID and frequency-aligned using the resonances of NAA, creatine, and choline. The two sub-FID's were subtracted to obtain an FID of the edited GABA signal, and for inspection of subtraction quality were Fourier-transformed. If patients moved during any of the GABA editing scans, the much larger and sharper Cr and Cho resonances caused well-defined subtraction errors that prevented the measurement of GABA, and any pairs of sub-spectra with such patient movement was not processed further. The remaining, good-quality pairs were used to determine the area of the GABA resonance at 3ppm from the differences using LCModel (45). LCModel was also applied to an averaged subspectrum from each measurement to determine the area of the resonance of creatine that lies at 3ppm, in addition to resonances of glutamate and glutamine. The concentration of GABA was determined from the ratio of GABA and total creatine resonances according to the equation [GABA] = $GABA_{LCModel}/Cr_{LCModel}$ x [Cr]. Assuming a creatine concentration varying linearly from 6 to 9 mM/kg wet weight with tissue type (46), the concentrations of GABA, glutamate, and glutamine, NAA and choline were calculated from the concentration of creatine determined for the measured tissue composition. The resonance areas of GABA, and the other metabolites were also measured as fractions of the resonance area of the unsuppressed water peak as an additional outcome that was provided by the LCModel

software. Figures 4 and 5 exemplify spectra that were obtained after this analysis was performed.

Functional Magnetic Resonance Imaging

Functional magnetic resonance imaging (fMRI) was performed on a Siemens 1.5T Sonata scanner located at the Yale University School of Medicine. Subjects' heads were immobilized within a circularly polarized head coil by using a neck support, foam wedges, and a restraining band drawn tightly around the forehead. Prior to functional imaging, 20 axial-oblique anatomic images (TE (echo time), 11 ms; TR (repetition time), 420 ms; FOV (field of view), 20 x 20 cm; 6 mm slice thickness, no gap; 256 x256 x 1 NEX (number of excitations)) were prescribed parallel to the intercommissural line based on sagittal localizer images (TE, 7.7; TR, 500 ms; FOV, 25.6 cm; 5 mm slice thickness, no gap; 256 x 256 x 1 NEX). Activation images were collected using single shot, gradient echo, echo planar acquisitions (flip angle, 80 degrees; TE, 50 ms; TR, 2000 ms; FOV, 20 x 20 cm; 6 mm slice thickness, no gap; 64 x 64 x 1 NEX) at the same 20 slice locations used for anatomic images. High-resolution anatomical images were obtained for 3-D reconstruction (Sagittal MPRAGE acquisition, flip angle, 8 degrees; TE, 3.65 ms; TR, 2000 ms; FOV, 25.6 x 25.6 cm; 1 mm slice thickness, no gap; 256 x 256 x 1 NEX; 160 slices total).

fMRI Task

A cue—target identity task was employed in an event-related design that requires making a match/mismatch judgment with a button press. A picture cue is presented in the upper central portion of the display (e.g., a picture of a dog) and is replaced by another picture approximately every quarter of the imaging run. On each trial, participants

compare the picture with one of the following six types of stimuli: [1] high-frequency words, presented visually, [2] high-frequency words, presented auditorily; [3] pseudowords, presented visually, [4] pseudowords, presented auditorily; [5] consonant strings, presented visually and [6] words semantically-related to the cue, presented visually. The majority of trials (80%) are mismatches and only data from mismatch trials are included in analyses so that we can compare brain responses with a common (no) decision. Because picture cue remain on the screen for the duration of multiple trials, each new picture cue is treated as a trial condition and initially presented on the screen by itself, allowing sufficient time to model separately the evoked responses to processing of the picture cues. For the fMRI session, 1090 full-brain images were collected across 10 runs (3 min, 38 sec each); a total of 340 trials [240 'no'; 60 'yes'; 40 picture] were presented at jittered trial durations (4, 5, 6, 7 sec), with occasional longer durations (null trials). This results in 40 trials per condition for each of the six main stimulus types and 40 trials for the picture condition.

Data analysis was performed using software written in MATLAB (MathWorks, Natick, MA). Images were first corrected for motion with SPM-99 (47) and sinc-interpolated to correct for slice acquisition time. For single-subject event-related analysis, a regression-based method was used, which allows direct estimation of the hemodynamic response for each trial type, at each voxel separately, without prior specification of a reference function (48, 49). Time course estimates were made for 1-sec intervals from -3 to +15 sec relative to trial onset. To create subject activation maps of the evoked response for each condition, we obtained regression estimates of the mean difference in these time course estimates for an activation period (3–8 sec after trial

onset) relative to a baseline period (0–3 sec prior to trial onset). Linear contrasts for effects of interest, including the evoked response of each trial type, simple subtractions among trial types, main effects, and interactions, were applied to these regression estimates to obtain contrast images for each subject. Across subjects, each voxel in these contrast images was tested versus zero with an F-test, implementing a mixed-model or repeated measures ANOVA (50, 51, 52). Prior to across-subjects analysis, anatomic images and subject activation maps were transformed into a common proportional three-dimensional grid (53), first by in-plane transformation and then by slice interpolation into the ten most superior slices of Talairach space, centered at z = +69, +60, +51, +42, +33, +23, +14, +5, -5, and -16 mm.

RESULTS

The GABA levels from an occipital region of interest (ROI) (see Figure 3) as measured using MRS, ranged from a minimum of 1.619mM/kg to a maximum of 2.128mM/kg (n=18). The mean GABA level was 1.823mM/kg with a standard deviation (SD) of 0.135 mM/kg. NAA levels from the same ROI ranged from a minimum of 12.840mM/kg to a maximum of 17.000 mM/kg (n=18). The mean NAA level was 14.762mM/kg with a standard deviation (SD) of 1.296. Table 1 provides the GABA, NAA levels and fMRI BOLD-activation scores for each of the 18 participants. There was a significant positive correlation between MRS-measured GABA and NAA levels in the occipital ROI, with a Pearson's correlation of 0.479 ($p<0.05$, 2-tailed, n=18), as shown in figure 6.

Figure 7 shows a color map of the composite fMRI BOLD response to a picture task in the 18 subjects. There is notable activation in slices 12-19 in the midline of the occipital lobe. This area includes the anterior aspect of the lingual gyrus in the occipital lobe, with possible involvement of the posterior cingulate gyrus. There is also significant activation in a variety of brain regions, including the thalami, the lateral occipital gyri, posterior middle and superior temporal gyri, the inferior frontal gyrus bilaterally and the anterior cingulate gyrus.

Figure 8 is a correlation map between GABA as measured by MRS and fMRI BOLD activation during picture processing in the midline of the occipital lobe. Using a Pearson's correlation statistical analysis, a significant positive correlation ($R=0.610$, $p=0.007$, 2-tailed) was found between GABA levels and fMRI BOLD activation scores in more superior slices of the occipital lobe, presented as a scatter plot in figure 9. The ROI

is slightly superior to the ROI used in the MRS study. It includes the superior aspect of the occipital lobe and spans slices +16 to +21 (on z-axis of Talairach coordinate system), with an ROI volume of 26,484mm^3 (i.e. 3.125mm by 3.125mm by 6mm and 452 functional voxels) and radius of 18.75mm. Other brain regions that demonstrate GABA and fMRI BOLD correlation include the thalamus bilaterally, the right posterior superior and middle temporal gyri, the inferior parietal lobule, the right superior frontal gyrus and the posterior cingulate gyrus.

NAA also demonstrated a strong correlation with fMRI BOLD activation in the occipital lobe as seen in the color map representation in figure 10. Using an ROI in more inferior slices of the occipital lobe that was slightly posterior to the MRS ROI, significant correlations (R=0.553, p=0.017, 2-tailed) are demonstrated in a scatter plot in Figure 11. The inferior slices span slices +7 to +11, with an ROI volume of 19,863mm^3 (i.e. 3.125mm by 3.125mm by 6mm and 339 functional voxels) and radius of 18.75mm. Other brain regions with BOLD and NAA correlation include the thalami bilaterally, the right inferior parietal lobule, and the left lateral occipital gyrus.

The correlations obtained in Figures 9 and 11 utilized ROIs for the fMRI activation that were from a slightly different part of the occipital lobe compared with the ROI used for the MRS study. We then used an ROI to obtain fMRI BOLD scores that was similar to the occipital ROI used in the MRS study. Significant correlations were also found between both GABA (Figure 12) and NAA (Figure 13) levels and BOLD activation scores during picture processing in the region approximating the MRS ROI (59,590mm^3 volume [i.e. 3.125mm by 3.125mm by 6mm and 1,017 functional voxels] and 18.75mm radius expanding from slices +7 to +21). For GABA, the Pearson's

correlation was 0.477 ($p=0.045$, 2-tailed), and for NAA the Pearson's correlation was 0.587 ($p=0.01$, 2-tailed). No correlation was seen between BOLD activation and glutamate or choline.

DISCUSSION

The present study investigated the interactions between MRS-measured metabolite levels and fMRI-BOLD activation in response to a picture-processing task performed on separate days and on different magnetic resonance systems. The findings indicate a positive correlation between GABA and NAA levels with fMRI BOLD activation, not only in the midline occipital ROI, but also in other regions of the brain. These results demonstrate that a major neurotransmitter, GABA, and a metabolite important to mitochondrial function in neurons, NAA, are linked to brain activation in children as they perform a cognitive task. As significantly more studies have been conducted using fMRI to study reading disability, this MRS-fMRI relationship also serves as an important validation for the role of future MRS studies in dyslexia and other cognitive processes.

GABA and Learning

The neurotransmitter measured in this study, GABA, is a widely distributed neurotransmitter in the central nervous system, with about sixty to eighty percent of neurons having GABA receptors. GABA is the major inhibitory neurotransmitter in the brain, and together with glutamate - the major excitatory neurotransmitter, act to regulate general brain activation. It is important to note that although GABA is viewed as an inhibitory neurotransmitter, neurons that produce GABA (GABAergic neurons) may have complex effects following activation. For instance, inhibitory neurons may be organized to provide negative feedback, leading to oscillatory interactions and the final effect of GABAergic neurons may be disinhibition. Inhibitory interneurons, by controlling the precise timing of firing of target cells, may also act to synchronize activity

among different neuronal populations (54). GABAergic neurons have been shown to participate in higher order CNS functions including learning, memory, emotions, etc. It is recognized as playing a significant role in the generation of coherent neural networks, exemplified by the fact that the visual cortex (the dominant sensory input area) has about fifty percent more GABA neurons than other cortical areas. GABAergic neurons have also been implicated in playing a role in neuronal plasticity in response to functional changes. For instance Floyer-Lea et al. (55) using MRS found that motor sequence learning in humans significantly decreased GABA concentration by almost 20% in the contralateral primary sensorimotor cortex within a 2 x 2 x 2-cm3 voxel. Enzymes involved in GABA synthesis were also altered in mouse cortex following sensory learning in a study by Gierdalski et al. (56). In humans, benzodiazepines (GABA receptor antagonists) are mainly used as anticonvulsants and anxiolytics, but manifest memory impairment as a side effect.

The role of GABA in learning and memory is also modeled in animal experiments, where benzodiazepines have been shown to impair spatial learning and memory (57). And these deficits have been successfully reversed by flumazenil, a benzodiazepine antagonist (58). Other studies in rats have shown that inverse agonists at specific GABA receptor subtypes enhance learning and memory (59, 60). Clinically, Piracetam (a cyclic derivative of GABA) has been documented to improve various cognitive impairments (61), including reading disabilities. Given the extensive indirect evidence, among other researchers, the authors involved in this study have proposed that a balance in excitatory and inhibitory neural impulses in specific regions in the brain is necessary for successful development of reading skills. And there is evidence to suggest

that the concentration of GABA in the cerebral cortex may be reflective of inhibitory neuron function, especially given that diseases such as depression, alcohol withdrawal and epilepsy, which alter GABA concentration also significantly affect inhibitory neural impulses in the brain (62, 63). In a separate arm of this study, the authors also test the hypothesis that polymorphisms of GABA-related genes may manifest in differences in GABA concentration in posterior language-related areas.

The development of non-invasive measurement of GABA levels using MRS has been critical in investigating the link between GABA concentration and inhibitory neuronal function, and subsequently exploring how this link may relate to reading disorders. However, GABA is difficult to measure in vivo using MRS for several reasons, including the fact that its small coupled spectral peaks are overlapped by much more intense resonances due to N-acetyl aspartate (NAA), creatine (Cr), and glutamate and glutamine (Glx) (27), resulting in increased complexity of the spectral analysis. And although methods to edit out these other signals have been developed (in our study we used a selective inversion pulse), the separation of coupled from uncoupled resonances is not absolute. Various studies have nevertheless established the feasibility of GABA detection and measurement using MRS including, Oz's group (64) who used a 4T magnet, STEAM MRS and LCModel to measure 10 metabolites, including GABA from the unilateral substantia nigra. The GABA/Glu ratio they obtained in the substantia nigra compared to the cortex, was in excellent agreement with established neurochemistry (in post-mortem studies). Other studies using MRS to measure GABA levels have included one by McLean et al. (27), where the authors successfully measured in vivo levels of GABA and established a control range of GABA levels in the occipital lobes of volunteer

participants; Epperson et al. (66) - found GABA levels to be reduced in post-partum women in the occipital cortex, compared to age matched controls; Floyer-Lea's group (55) - studied alterations in GABA concentration following motor learning. The GABA range obtained in the current study (1.619mM/kg to a maximum of 2.128mM/kg) is in reasonable agreement with ex-vivo measurements of human cerebral GABA with concentration as high as 2.1mM/kg (66).

GABA and fMRI

Since its use in human experiments in the 1990s, several studies have been conducted to investigate the mechanism of the fMRI BOLD phenomenon. In general, these studies have concluded that fMRI does not directly measure neuronal activity, but relies on a signal, which results from changes in oxygenation, blood volume and flow – hence BOLD (blood oxygen level demand). Neurons require energy in other to maintain and restore membrane potentials that is necessary for signaling. The primary source of energy for the brain is ATP created from glucose and oxygen, which are not stored in the brain and have to be replenished by continuous blood supply. Therefore increases in neuronal activity result in increase in local energy demand, which results in increase in blood flow. In other words, it is actually the metabolic demands of active neurons that are measured indirectly by fMRI (67). The metabolic demands of increased neuronal activity lead to an increase in oxygenated blood primarily from increased blood flow. More oxygen is supplied to the area than is extracted. This results in a decrease in the amount of deoxygenated hemoglobin in the active brain region. Oxygenated hemoglobin does not dephase protons in contrast to deoxygenated hemoglobin, which results in dephasing and signal loss. The MR signal of a brain region during a task compared to a

baseline condition will therefore increase due to its relative increase in oxyhemoglobin compared with deoxyhemoglobin.

The finding of a positive correlation between GABA and fMRI BOLD in response to the picture processing task in the current study provides evidence for the role of GABA in cognitive processes. Interestingly, ^{13}C MRS studies in rats and humans have shown a one-to-one relationship between the metabolism of glucose in the tricarboxylic acid cycle and the cycling of neurotransmitters including GABA, which is released by neuronal firing and cycled via astrocytes through glutamine. There is also a one-to-one relationship between the rate of glucose oxidation and neuronal firing. Putting these together, it may be that the brain regions with appropriately developed GABAergic neuronal activity are capable of optimal functioning in response to cognitive tasks. This is evidenced by the correlation of increased GABA levels with increased fMRI BOLD signal. As discussed previously, Shaywitz et al. (5) have shown that higher reading skill correlates with stronger BOLD activation in the left hemisphere ventral cortex. Thus although GABA levels were not studied in relation to reading skill in the current study, this result suggests, albeit tentative that such a relationship may exist.

NAA and Neuroenergetics

As discussed in the introduction, NAA is an indirect measure of neuronal integrity. The results in the current study found that higher NAA levels correlated with higher regional blood oxygen demand in the occipital MRS-ROI during a task. The correlation of NAA and BOLD is supported by a study demonstrating that compared to healthy controls, schizophrenic patients tend to have low NAA levels in the prefrontal

cortex, which correlate with significantly lower increase in blood flow during cognitive tasks (68).

A potential for NAA use clinically has been raised by studies showing that NAA appears to be reduced in bipolar disorder (a disorder with mood and cognitive deficits), and lithium (an effective treatment for bipolar disorder) has been reported to increase NAA levels. Other clinical uses for NAA include the evaluation of diseases that destroy or injure neurons, like neoplasms, infection, stroke, demyelination or trauma. These processes can lead to marked decreases in NAA levels.

In general, NAA is widely used as a neuronal "marker" because of its relatively high concentration in neurons and its generation of a readily visible single peak on NMR spectra. Increased NAA levels are generally believed to represent an increased number of intact neurons. However, the MRS-fMRI relationship seen with NAA may be more complex, given the potential role of NAA in metabolism, neuroenergetics and ultimately cognitive processes. Shulman & Rothman (69) summarized from studies in their book that although the exact biological function of NAA is still unknown, its slow leak and small quantity release from neurons is inconsistent with a neurotransmitter function. One author proposed that NAA aids transportation of water across the hydrophobic myelin sheath during axonal firing (74), enabling more rapid and synchronized neuronal conduction, and thus better cognitive performance (21). As an indicator of neuronal integrity, a study (70) demonstrated that NAA not only correlates with neuronal loss in animal models of stroke, but also with neuronal dysfunction. NAA's role in energy metabolism and brain function is supported by the fact that it is synthesized by a mitochondrial enzyme (71). Animal experiments have shown a significant correlation

between ATP loss and NAA levels following traumatic brain injury, consistent with a role for NAA in neuroenergetics (72). In addition, O'Neill et al's (73) PET/MRS study demonstrated a positive correlation between the *in vivo* rate of glucose utilization and the level of NAA. The fact that the fMRI-BOLD signal is indirectly reflective of energy metabolism and NAA has also been implied in neuroenergetics suggests a key relationship. In summary, the current study demonstrates that the fMRI signal during a task is directly correlated with NAA, which is a marker of neuronal function and is involved in neuronal energy metabolism. NAA levels thus appear to be important for brain function during cognitive tasks.

GABA-NAA Relationship

An explanation for the positive correlation between GABA and NAA (Figure 6) is the fact that as presented above, NAA has been shown to correlate with neuronal volume. Therefore, areas of the brain with increased GABAergic neuronal density will be expected to have increased NAA levels and vice-versa. However, NAA is more directly implicated in glutamate cycling. But glutamate is also a GABA precursor and NMR studies indicate that GABA and glutamine cycling is an important part of GABA production. Through its role in mitochondrial energetics in glutamine cycling, NAA may be an indirect correlate of GABA neurotransmitter production and release.

This is also suggested in epilepsy studies, where brain regions involved in epilepsy have lower NAA levels, indicating suboptimal mitochondrial energetic function. There is also increased extracellular glutamate and a decreased rate of glutamate recycling.

Conclusion

The preliminary results obtained in this study indicate a significant correlation between metabolic and hemodynamic measures in cognitive processes using two important magnetic resonance diagnostic modalities, MRS and fMRI. The results also support the potential role for GABA in reading (dis)ability, which has important implications for understanding the pathophysiology and also in drug development and research. It also raises the possibility for the role of NAA as an adjunct in fMRI studies and as a potential biomarker in cognitive disorders. It is important to conduct additional studies in this area to further explore and confirm these findings.

REFERENCES

1. World Health Organization. ICD-1. http://www.who.int/classifications/apps/icd/icd10online 2006. (Accessed 11 Jan. 2007)
2. Tunmer, W.E., and Nesdale, A.R. 1985. Phonemic segmentation skill and beginning reading. *Journal of Educational Psychology*. 77:417-427.
3. Wagner, R.K., and Torgesen, J.K. 1987. The nature of phonological processing and its causal role in the acquisition of reading skills. *Psychological Bulletin*. 101:192-212.
4. Penolazzi, B., Spironelli, C., Vio, C., and Angrilli, A. 2006. Altered hemispheric asymmetry during word processing in dyslexic children: an event-related potential study. Neuroreport. 17(4):429-433
5. Shaywitz, B.A., Shaywitz S.E., Pugh, K., et al. 2002. Disruption of posterior brain systems for reading in children with developmental dyslexia. *Biological Psychiatry*. 52:101-110.
6. Georgiewa, P., Rzanny, R., Gaser, C., Gerhard, U.J., Vieweg, U., and Freesmeyer, D., et al. 2002. Phonological processing in dyslexic children: a study combining functional imaging and event related potentials. *Neurosci Lett*. 218:5–8
7. Breier, J.I., Simos, P.G., Fletcher, J.M., Castillo, E.M., Zhang, W., Papanicolaou A.C. 2003. Abnormal activation of temporoparietal language areas during phonetic analysis in children with dyslexia. *Neuropsychology*. 17(4):610-621.
8. Shaywitz, S.E., Shaywitz, B.A., Pugh, K.R., Fulbright, R.K., Constable, R.T., et al. 1998. Functional disruption in the organization of the brain for reading in dyslexia. *Proceedings of the National Academy of Sciences of the United States of America.* 95(5):2636-2641.
9. Paulesu, E., Frith, U., Snowling, M., et al. 1996. Is developmental dyslexia a disconnection syndrome? Evidence from PET scanning. *Brain* 119:143–157.
10. Brambati, S.M., Termine, C., Ruffino, M., Stella, G., Fazio, F., et al. 2004. Regional reductions of gray matter volume in familial dyslexia. *Neurology*. 63(4):742-725.
11. Eckert, M.A., Leonard, C.M., Richards, T.L., Aylward, E.H., Thomson, J. et al. 2003. Anatomical correlates of dyslexia: frontal and cerebellar findings. *Brain*. 126(2):482-94.
12. Galaburda, A.M. 1993. Neuroanatomical basis of developmental dyslexia. *Neurologic Clin*. 11:161–173.
13. Francks, C., Paracchini, S., Smith, S.D., Richardson, A.J., Scerri, T.S., et al. 2004. A 77-kilobase region of chromosome 6p22.2 is associated with dyslexia in families from the United Kingdom and from the United States. *American Journal of Human Genetics*. 75(6):1046-1058
14. de Kovel, C.G. Hol, F.A., Heister, J.G., Willemen, J.J., Sandkuijl, L.A., et al. 2004. Genomewide scan identifies susceptibility locus for dyslexia on Xq27 in an extended Dutch family. *Journal of Medical Genetics*. 41(9):652-657

15. Cope, N., Harold, D., Hill, G., Moskvina, V., Stevenson, J., et al. 2005. Strong evidence that KIAA0319 on chromosome 6p is a susceptibility gene for developmental dyslexia. *American Journal of Human Genetics*. 76(4):581-591
16. Brambati, S.M, Termineb, C., Ruffinoa, M, Dannae, M., and Lanzif, G. 2006. Neuropsychological deficits and neural dysfunction in familial dyslexia. *Brain research.* 1113 (1):174 –185
17. Rae, C., Lee, M.A., Dixon, R.M., Blamire, A.M., Thompson, C.H. et al. 1998. Metabolic abnormalities in developmental dyslexia detected by 1H magnetic resonance spectroscopy. *Lancet*. 351:1849-1852.
18. Richardson, A.J., Cox, J., Sargentoni, J., and Puri, P.K. 1997. Abnormal Cerebral Phospholipid Metabolism in Dyslexia Indicated by Phosphorus-31 Magnetic Resonance Spectroscopy. *NMR in Biomedicine*.10: 309–314
19. Richards, T.L., Dager, S.R., Corina, D., Serafini, S., Heide, A.C., et al. 1999. Dyslexic Children Have Abnormal Brain Lactate Response to Reading-Related Language Tasks. Am J Neuroradiol 20:1393–1398
20. Richards, T.L., Berninger, V.W., Aylward, E.H., Richards, A.L., Thomson, J.B., et al. 2002. Reproducibility of Proton MR Spectroscopic Imaging (PEPSI): Comparison of Dyslexic and Normal-Reading Children and Effects of Treatment on Brain Lactate Levels during Language Tasks. *Am J Neuroradiol.* 23: 1678-1685.
21. Jung, R.E., Haier, R.J., Yeo, R.A., Rowland, L.M., Petropoulos, H., et al. 2005. Sex differences in N-acetylaspartate correlates of general intelligence: An 1H-MRS study of normal human brain. *Neuroimage*. 26:965-972.
22. Winblad, B. 2005. Piracetam: a review of pharmacological properties and clinical uses. *CNS Drug Reviews*. 11(2):169-182.
23. Grigorenko, E.L. 2003. The first candidate gene for dyslexia: Turning the page of a new chapter of research. *Proc Natl Acad Sci* 100(20): 11190–11192.
24. Thiel, C.M., Henson, R.N., Morris, J.S., Friston, K.J., and Dolan, R.J. 2001. Pharmacological modulation of behavioral and neuronal correlates of repetition priming. *J Neurosci*. 21(17): 6846-6852.
25. Goei, V. L., Choi, J. A., Bowlus, C.L., Raha-Chowdhury, R., and Gruen, J. R. 1998. Human gamma-aminobutyric acid B receptor gene: complementary DNA cloning, expression, chromosomal location, and genomic organization. *Biological Psychiatry*. 44(8):659-666.
26. Hisama, F. M., Gruen, J.R., Choi, J., Huseinovic, M., Grigorenko, E.L., et al. 2001. Human GABA(B) receptor 1 gene: eight novel sequence variants. *Human Mutation*. 17(4):349-350.
27. McLean, M.A., Busza, A.L., Wald, L.L., Simister, R.J., Barker, G.J. et al. 2002. In vivo GABA+ measurement at 1.5T using a PRESS-localized double quantum filter. *Magn Reson Med.* 48(2): 233-241
28. Shaywitz, B. A., Lyon, G. R., and Shaywitz, S. E. 2006. The role of functional magnetic resonance imaging in understanding reading and dyslexia. *Developmental neuropsychology*. 30 (1):613 – 632
29. Chen, M.Y., Pope, T.L. 2004.. *Basic Radiology*. McGraw-Hill Companies. <http://www.accessmedicine.com/resourceTOC.aspx?resourceID=75> 2006. (Accessed online 07 Feb. 2007)

30. Mukherji, S.K. 1998. Clinical Applications of MR spectroscopy. John Wiley & Sons.
31. Salibi N., and Brown M.A. 1997. Clinical MR spectroscopy. Wiley-Liss.
32. Thulborn, K.R. and Davis, D. 2001. Clinical Applications of fMRI. In *Current Protocols in Magnetic Resonance Imaging*. <http://www.mrw.interscience.wiley.com/emrw/9780471142713/cp/cpmi/article/mia0601/current/abstract>Accessed 08 Feb. 2007
33. Hongyu, A., and Weili, L. 2005. Basic Spin Properties and the Bloch Equations. In *Current Protocols in Magnetic Resonance Imaging*. John Wiley & Sons. <http://www.mrw.interscience.wiley.com/emrw/9780471142713/cp/cpmi/article/mib0300/current/abstract> Accessed 08 Feb. 2007
34. Weili, L. 2005 Spin and Gradient Echoes. In *Current Protocols in Magnetic Resonance Imaging*. John Wiley & Sons. <http://www.mrw.interscience.wiley.com/emrw/9780471142713/cp/cpmi/article/mib0401/current/abstract>Accessed 08 Feb. 2007
35. Wechsler, D. 1991. *Wechsler Intelligence Scale for Children*. Third Edition. Psychological Corporation
36. Woodcock, R.W., and Johnson, M.B. 1989. *Woodcock-Johnson Psycho-educational Battery–Revised*. Chicago, IL: Riverside.
37. Fletcher, J. M., Shaywitz, S. E., Shankweiler, D., Katz, L., Liberman, I., Stuebing, K., Francis, D. J., Fowler, A., and Shaywitz, B. A. 1994. Cognitive profiles of reading disability: Comparisons of discrepancy and low achievement definitions. *J. Educ. Psychol*. 86: 6–23.
38. Siegel, L. S. 1989. IQ is irrelevant to the definition of learning disabilities. *J. Learn. Disab*. 22: 469–479.
39. Stanovich, K. E., and Siegel, L. S. 1994. The phenotypic performance profile of reading-disabled children: A regression-based test of the phonological-core variable-difference model. *J. Educ. Psychol*. 86: 24–53.
40. Rothman, D.L, Petroff, O.A, Behar, K.L, & Mattson, R.H. 1993. Localized ^{1}H NMR measurements of gamma-aminobutyric acid in human brain in vivo. *Proceedings of the National Academy of Sciences of the United States of America*. 90(12):5662-6
41. Hetherington, H.P., Pan, J.W., Mason, G.F., Adams, D., Vaughn, M.J., et al. 1996. Quantitative 1H spectroscopic imaging of human brain at 4.1 T using image segmentation. *Magnetic Resonance in Medicine*. 36(1):21-29
42. Mason, G.F., Chu, W.J., and Hetherington, H.P. 1997. A general approach to error estimation and optimized experiment design, applied to multislice imaging of T1 in human brain at 4.1 T [published erratum appears in *J Magn Reson* 1997. 127(1):134-6]. *Journal of Magnetic Resonance*. 126(1):18-29.
43. Silver, M.S., Joseph, R.I., Chen, C.N., Sank, V.J., and Hoult, D.I. 1984. Selective population inversion in NMR. *Nature*. 310(5979):681-683
44. Mason, G.F. 2002. Graded Image Segmentation of Brain Tissue in the Presence of Inhomogeneous Radio Frequency Fields. *Magn Reson Imaging*. 20:431-436

45. Provencher, S.W. 1993. Estimation of metabolite concentrations from localized *in vivo* proton NMR spectra. *Magn Reson Med*. 30:672-679
46. Michaelis, T., de Biurrun, G., Watanabe, T., Frahm, J., Ohl, F., and Fuchs, E. 2001. Gender-specific alterations of cerebral metabolites with aging and cortisol treatment. J Psych Res. 35:231-237
47. Friston, K. J., Ashburner, J., Frith, C., Poline, J.B., Heather, J., and Frachowiak, R. 1995. Spatial registration and normalization of images. *Hum. Brain Map*. 2:165–189
48. Miezin, F. M., Maccotta, L., Ollinger, J. M., Peterson, S. E., and Buckner, R. L. 2000. Characterizing the hemodynamic response: Effects of presentation rate, sampling procedure, and the possibility of ordering brain activity based on relative timing. *NeuroImage* 11:735–759
49. Ollinger, J. M., Shulman, G. L., and Corbetta, M. 2001. Separating processes within a trial in event-related functional MRI. I. The method. *NeuroImage* 13: 210–217.
50. Holmes, A.P, and Friston, K.J.1998. Generalizability, random effects, and population inference. *Neuroimage* 7:S34
51. Kirk, R.E. 1982. *Experimental design: procedures for the social sciences*. Wadsworth, Belmont, CA
52. Woods, R.P. 1996. Modeling for intergroup comparisons of imaging data. *Neuroimage* 4:S84–S94
53. Talairach, J and Tournoux, P. *Co-Planar Stereotaxic Atlas of the Human Brain*. Thieme, Stuttgart, Germany.
54. Webster, R. (editor). 2001. *Neurotransmitters, Drug and Brain Function*. John Wiley & Sons.
55. Floyer-Lea, A., Wylezinska, M., Kincses, T., Matthews, P.M. 2006. Rapid modulation of GABA concentration in human sensorimotor cortex during motor learning. *Journal of Neurophysiology*. 95(3):1639-44
56. Gierdalski, M., Jablonska, B., Siucinska, E., Lech, M., Skibinska, A., & Kossut, M. 2001. Rapid regulation of GAD67 mRNA and protein level in cortical neurons after sensory learning. Cerebral Cortex, 11, 806-815.
57. Keith, J.R., Pitts, R.C., Pezzuti, T., and Galizio, M. 2003. Effects of positive GABA(A) modulators on a multiple-component, repeated-acquisition test of spatial learning. *Behavioural Pharmacology*. 14(1):67-75
58. Perry, E. (Editor). 2002. Neurochemistry of Consciousness. *Neurotransmitters in mind*. John Benjamins Publishing Company. <http://site.ebrary.com/lib/yale/Doc?id=10022353&ppg=127> (Accessed online on 04 March. 2007)
59. Getova, D. and Bowery, N,G. 1998. The modulatory effects of high affinity GABA(B) receptor antagonists in an active avoidance learning paradigm in rats. *Psychopharmacology*. 137(4):369-373.
60. Dawson, G.R., Maubach, K.A., Collinson, N., Cobain, M., and Everitt, B.J. et al. 2006. An inverse agonist selective for alpha5 subunit-containing GABAA receptors enhances cognition. *Journal of Pharmacology & Experimental Therapeutics*. 316(3):1335-45

61. Waegemans, T., Wilsher, C.R., Danniau, A., Ferris, S.H., Kurz, A., Winblad, B. 2002. Clinical efficacy of piracetam in cognitive impairment: a meta-analysis. 13(4):217-24
62. Petroff, O. A., Rothman, D. L., Behar, K. L., & Mattson, R. H. 1996. Low brain GABA level is associated with poor seizure control. *Annals of Neurology*, 40(6), 908-911.
63. Behar, K. L., & Rothman, D. L., Petersen, K. F., Hooten, M., Delaney, R., Petroff, O. A., Shulman, G. I., Navarro, V., Petrakis, I. L., Charney, D. S., & Krystal, J. H. 1999. Preliminary evidence of low cortical GABA levels in localized 1H-MR spectra of alcohol-dependent and hepatic encephalopathy patients. *American Journal of Psychiatry*, 156(6), 952-954.
64. Oz, G., Terpstra, M., Tkac, I., Aia, P., Lowary, J., et al. 2006. Proton MRS of the unilateral substantia nigra in the human brain at 4 tesla: detection of high GABA concentrations. *Magnetic Resonance in Medicine*. 55(2):296-301.
65. Epperson, C.N., Gueorguieva, R., Czarkowski, K.A., Stiklus, S., and Sellers, E. et al. 2006. Preliminary evidence of reduced occipital GABA concentrations in puerperal women: a 1H-MRS study. *Psychopharmacology*. 186(3):425-433.
66. Petroff, O.A., Pleban, L.A. & Spencer, D.D. 1995. Symbiosis between in vivo and in vitro NMR spectroscopy: the creatine, N-acetyl aspartate, glutamate, and GABA content of the epileptic human brain. *Magn Reson Imaging* 13: 1197-1211.
67. Huettel, A.S., Song, A.W., McCarthy, G. 2003. *Functional Magnetic Resonance Imaging*. Sinauer Associates.
68. Bertolino, A., Esposito, G., Callicott, J.H., Mattay, V.S. and Van Hownr, J.D., et al. 2000. Specific relationship between prefrontal neuronal N-acetylaspartate and activation of the working memory cortical network in scizophrenia. *Am J Psychiatr*. 157: 26-33
69. Shulman, R.G. & Rothman, D.L. [Editors] 2004. Brain energetics and neuronal activity: Applications to fMRI and Medicine. John Wiley & Sons, Ltd. pg 240-256.
70. Demougeot, C., Garnier, P., Mossiat, C., Bertrand, N., and Giroud, M. et al. 2001. N-Acetylaspartate, a marker of both cellular dysfunction and neuronal loss: its relevance to studies of acute brain injury. *Journal of Neurochemistry*. 77(2):408-415.
71. Patel, T.B., and Clark, J.B. 1979. Synthesis of N-acetyl-L-aspartate by rat brain mitochondria and its involvement in mitochondrial/cytosolic carbon transport. *Biochem. J*. 184: 539-546
72. Signoretti, S., Marmarou, A., Tavazzi, B., Lazzarino, G., Beaumont, A., Vagnozzi, R. 2001. N-Acetylaspartate reduction as a measure of injury severity and mitochondrial dysfunction following diffuse traumatic brain injury. *Journal of Neurotrauma*. 18(10):977-91.
73. O'Neill, J., Eberling, J.L., Schuff, N., Jagust, W. and Reed, B. 2000. Method to correlate 1H MRSI and 18FDG-PET. *Magn Reson* Med 43: 244-250

74. Baslow, M.H. 2002. Evidence supporting a role for N-acetyl-L-aspartate as a molecular water pump in myelinated neurons in the central nervous system. An analytical review. *Neurochemistry International*. 40(4):295-300
75. Mason, G.F, and Rothman, D.L (2002) Graded Image Segmentation of Brain Tissue in the Presence of Inhomogeneous Radio Frequency Fields. *Magn Reson Imaging* 20: 431-436

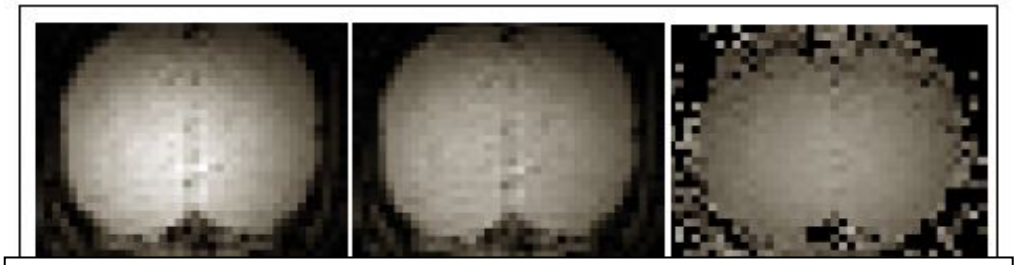

Figure 1. B_1 images. To image the RF inhomogeneity as a B_1 image, the two images are acquired with a delay of 51 ms between the two acquisitions using the same pulse angle (left and center). The 2nd image is proportional to the first by the cosine of the excitation angle. The pulse angle image can then be converted to an image of B_1 (far right). (75)

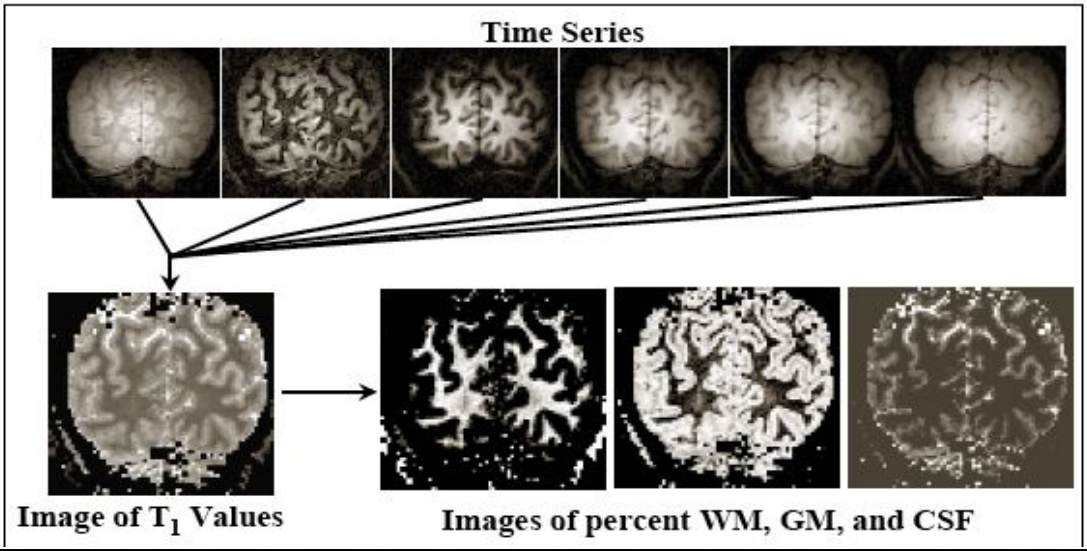

Figure 2. Imaging of T_1 and tissue type. After an inversion pulse is applied, a series of images is acquired to track the T_1 recovery of the water magnetization (top row). Least-squares fitting is performed using a numerical simulation of the pulse sequence to obtain an image of the T_1 values (instead of a T_1-weighted image) (bottom left). The T_1 values are used to determine the percentage of WM, GM, and CSF in each pixel (bottom right 3 images). (75)

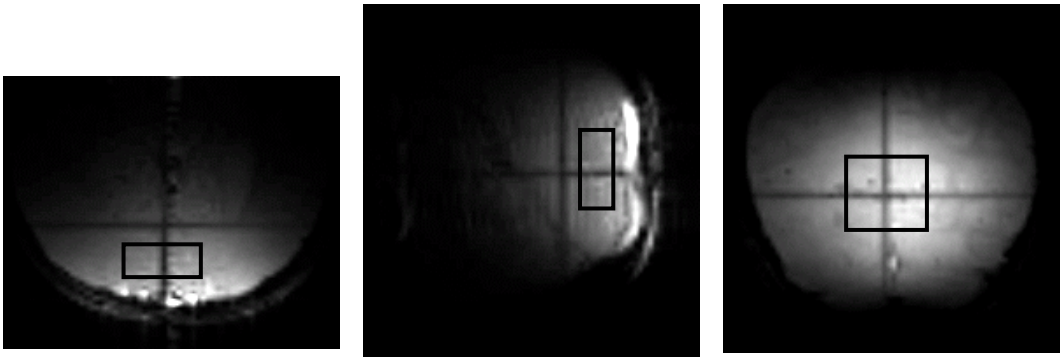

Figure 3: Localizer images in axial, sagittal and coronal planes demonstrating location of voxel used for MRS measurements. The voxel was 3 cm right to left, 3 cm superior to inferior and 1.5 cm anterior to posterior

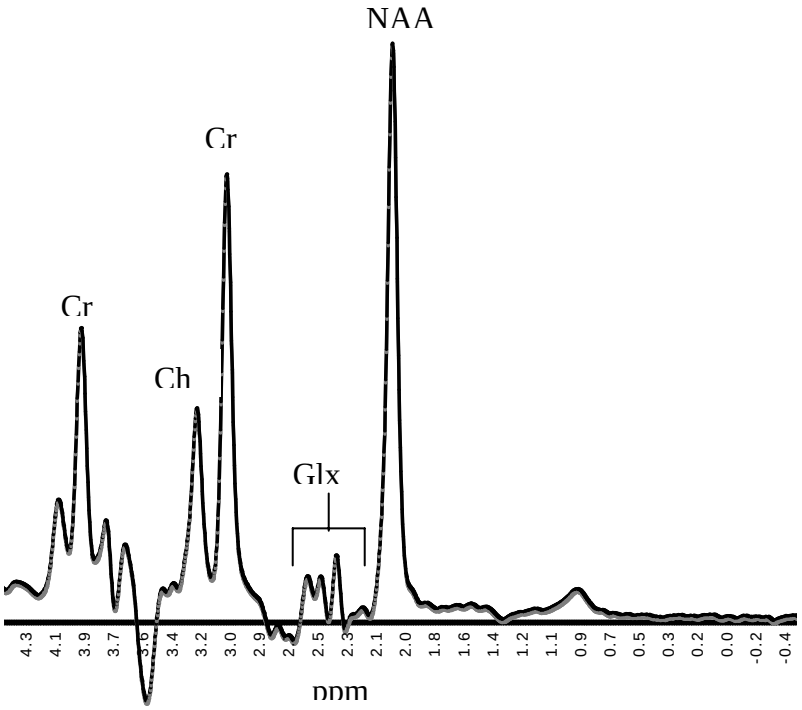

Figure 4: MRS measurements of brain metabolites. NAA, N-acetyl aspartate. Glx, glutamate and glutamine. Cr, creatine. Ch, choline.

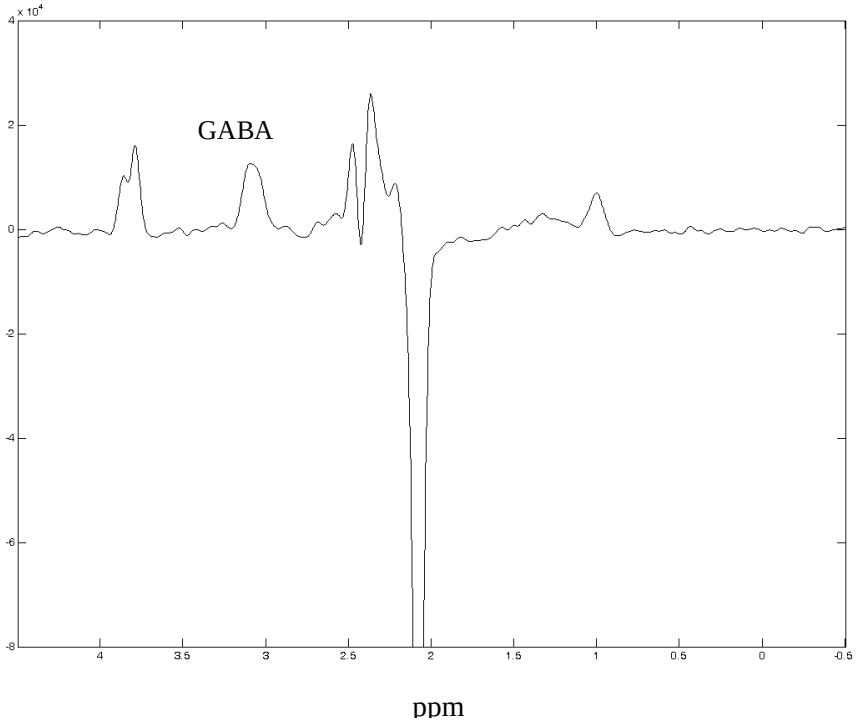

Figure 5: Cortical GABA detected by J-editing. GABA, gamma-aminobutyric

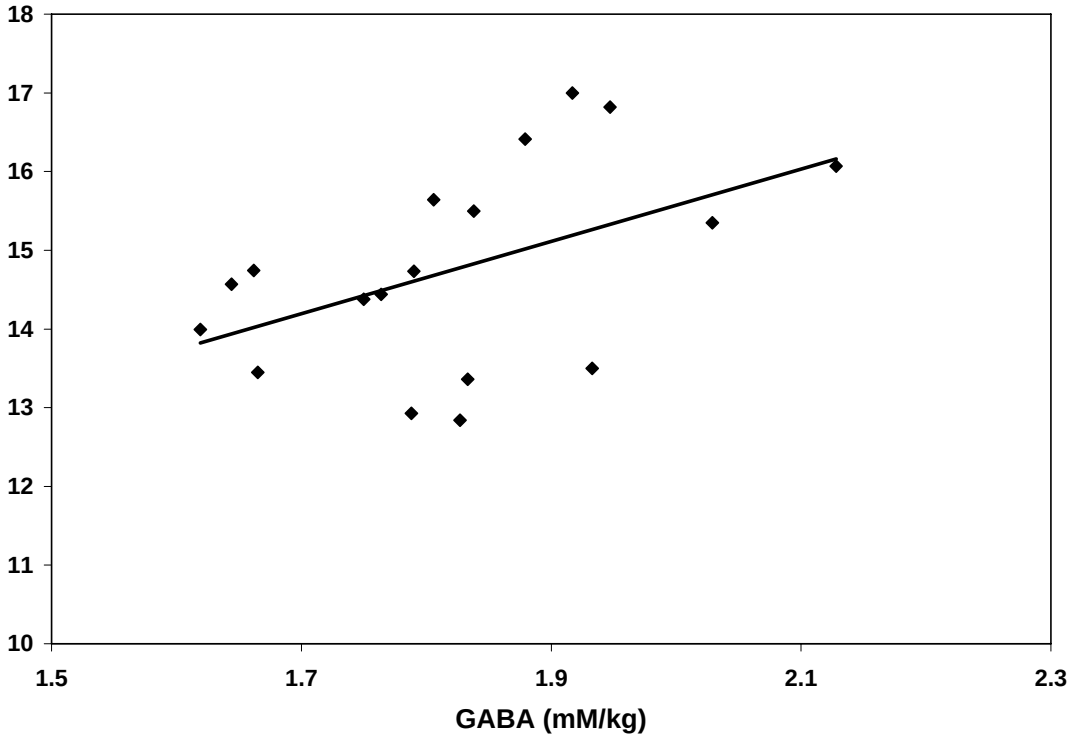

Figure 6: Correlation between MRS measured NAA and GABA levels from the occipital ROI of Figure 3. R=0.479 (p=0.044, 2-tailed, n= 18)

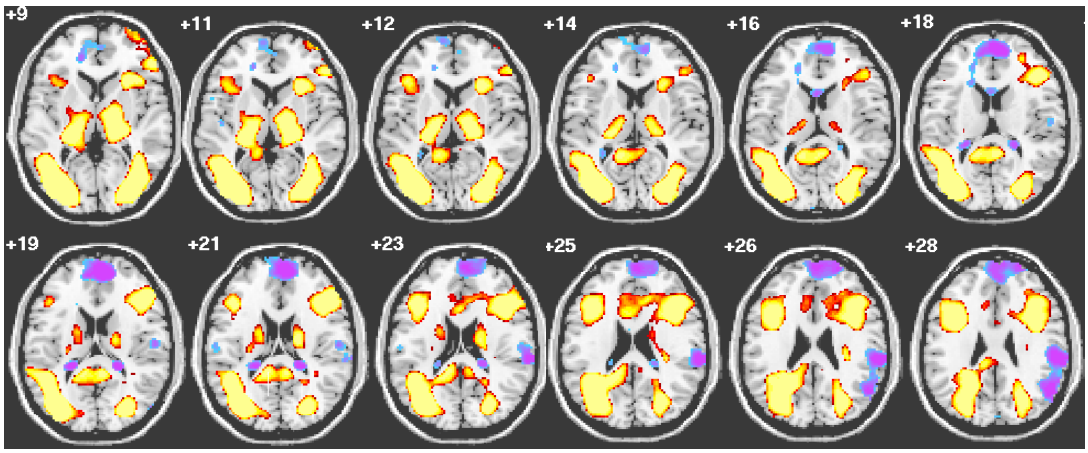

Figure 7. Composite fMRI BOLD response to pictures in 18 subjects., p = 0.05. Note activation in the midline of the lingual gyrus on slices 12-19.

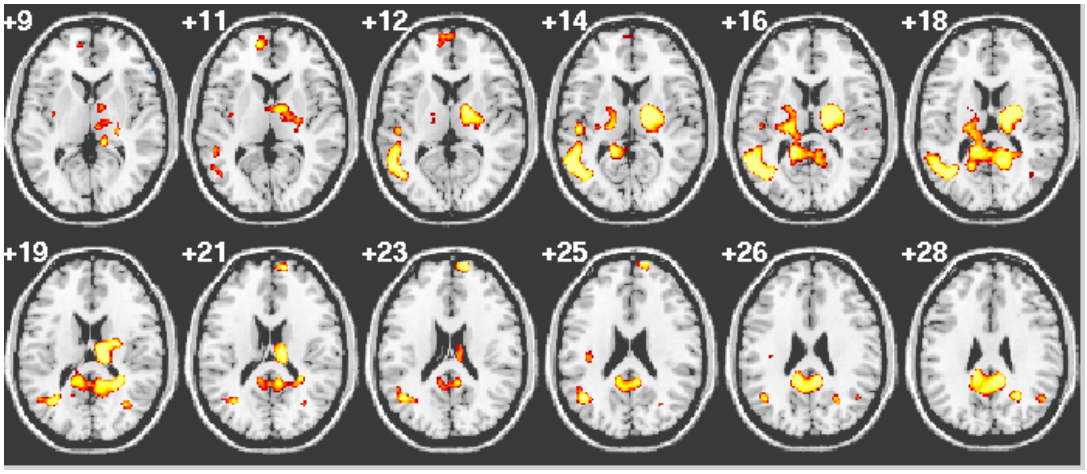

Figure 8: Correlation map between GABA levels and BOLD activation scores during picture processing. p<0.01, 2-tailed.

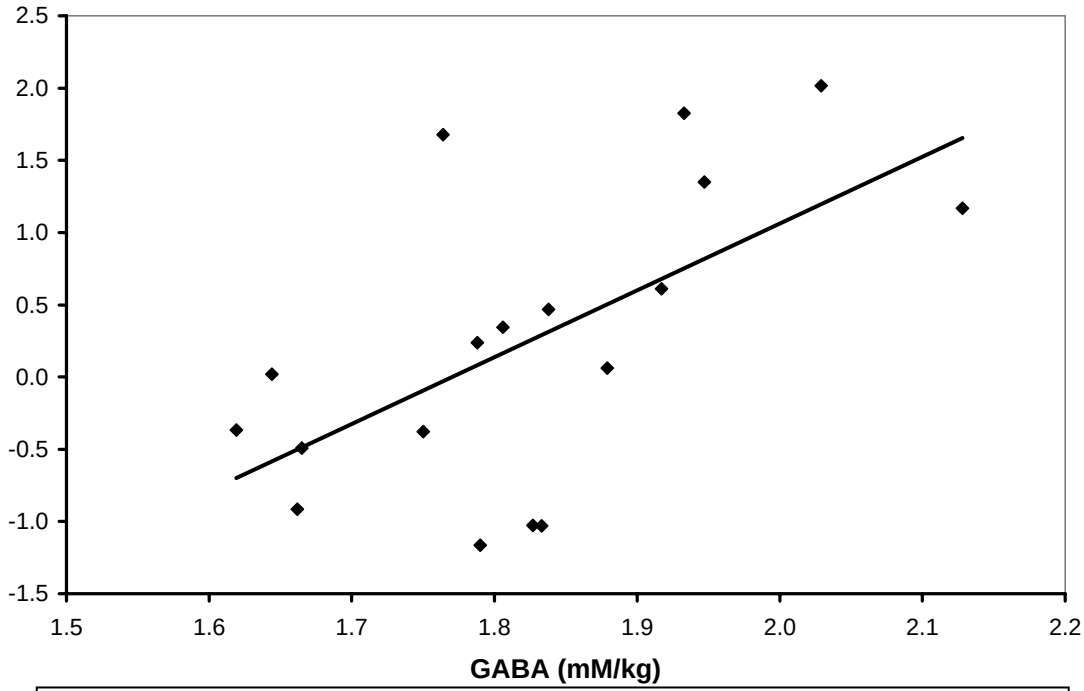

Figure 9: Correlation between GABA level and BOLD activation scores during picture processing using an occipital ROI placed in slices 16-21 in Figure 8. R=0.610, p=0.007, 2-tailed. ROI volume of 26,484mm3 and 18.75mm radius.

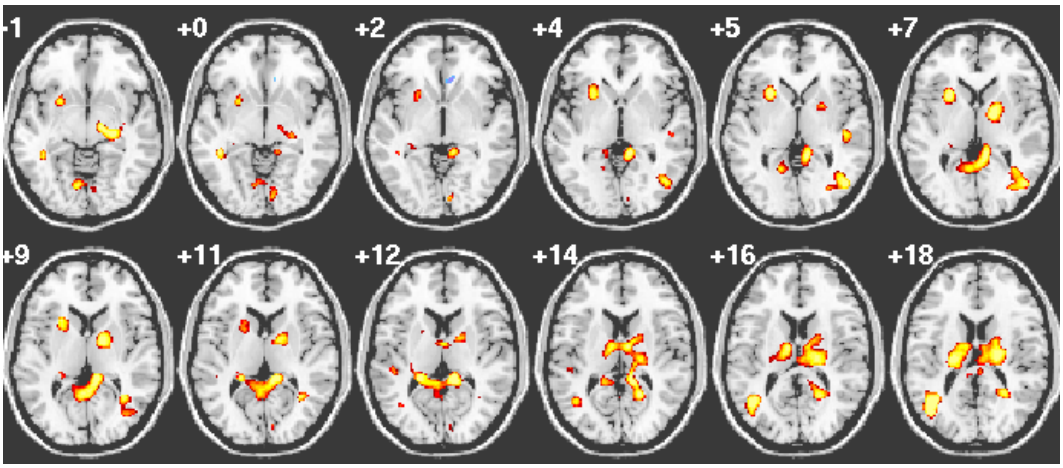

Figure 10: Correlation map between NAA levels and BOLD activation scores during picture processing. P<0.01, 2-tailed.

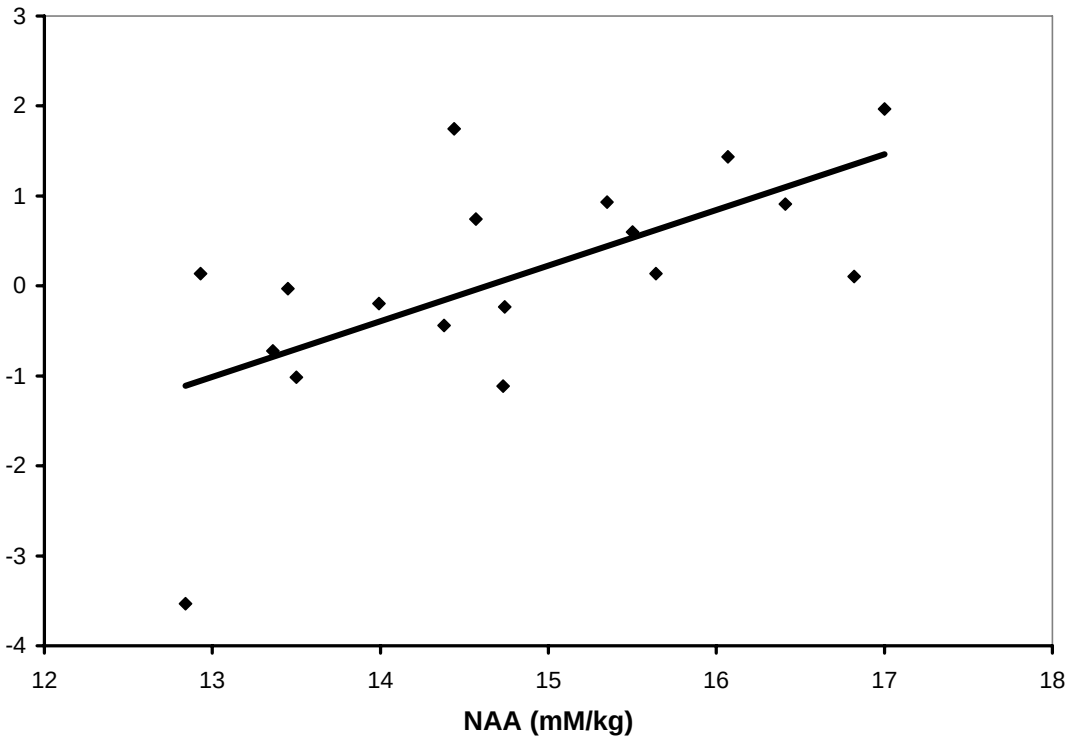

Figure 11: Correlation between NAA level and BOLD activation scores during picture processing using an occipital ROI placed in slices 7-12 in Figure 10. R=0.553, p=0.017, 2-tailed. ROI volume of 19,863mm3 and 18.75mm radius.

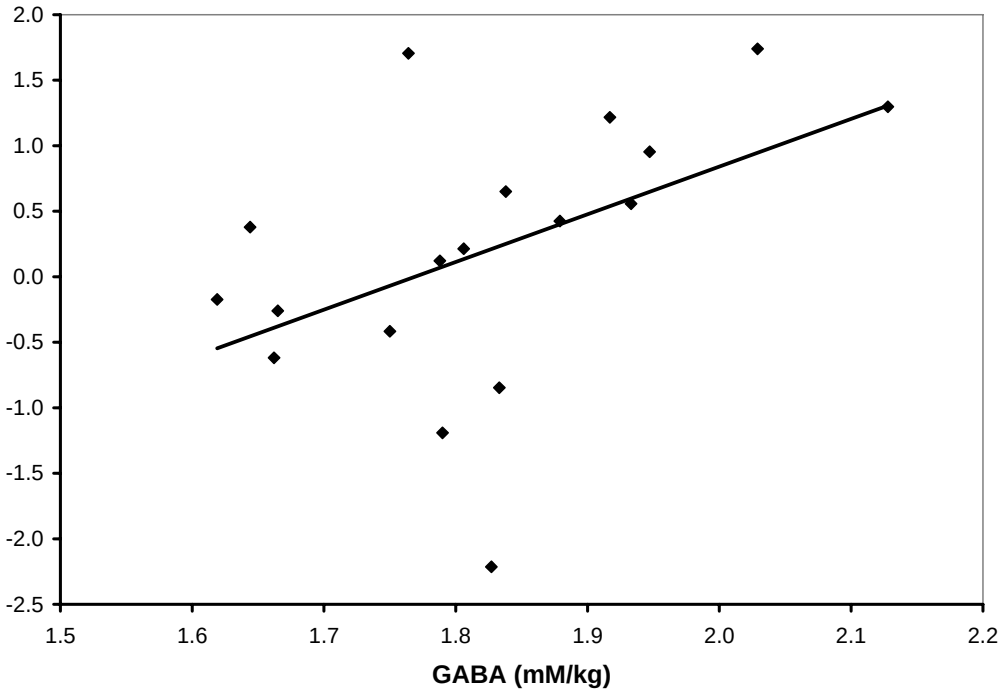

Figure 12: Correlation between MRS measured GABA levels and fMRI BOLD activation scores during picture processing from an occipital ROI similar to the MRS ROI in Figure 3. R=0.477 (p=0.045, 2-tailed). fMRI ROI = volume of 59,590mm3 and 18.75mm radius from slices +7 to +21.

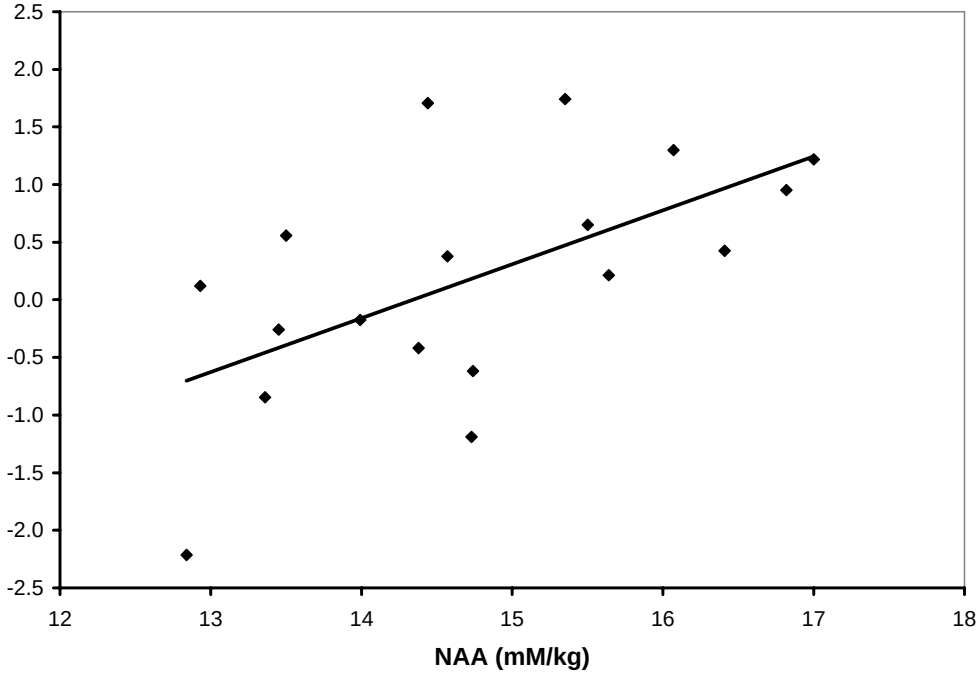

Figure 13: Correlation between MRS measured NAA levels and fMRI BOLD activation scores during picture processing from an occipital ROI similar to the MRS ROI in Figure 3. R=0.587 (p=0.01, 2-tailed). fMRI ROI = volume of 59,590mm3 and 18.75mm radius from slices +7 to +21.

Participant #	Gender	Age at fMRI testing (yr)	GABA (mM/kg)	NAA (mM/kg)	Superior slices BOLD	Inferior Slices BOLD	"MRS ROI" BOLD
1	M	8.0	2.128	16.07	1.166900	1.43390	1.29880
2	F	7.8	1.644	14.57	0.021051	0.74152	0.37761
3	F	8.3	1.788	12.93	0.238820	0.13621	0.12027
4	F	7.7	1.806	15.64	0.344680	0.13508	0.21367
5	F	8.2	1.838	15.50	0.467240	0.59854	0.65097
6	F	7.0	1.764	14.44	1.676600	1.74680	1.70540
7	M	6.8	1.662	14.74	-0.913770	-0.23254	-0.61759
8	F	8.4	1.947	16.82	1.350400	0.10265	0.95373
9	M	7.6	1.933	13.50	1.826600	-1.01470	0.55795
10	F	8.8	1.917	17.00	0.610750	1.96570	1.21730
11	M	10.3	1.879	16.41	0.060588	0.91072	0.42578
12	F	7.4	1.750	14.38	-0.377120	-0.43925	-0.41757
13	M	9.0	1.619	13.99	-0.366840	-0.19705	-0.17445
14	M	7.9	1.833	13.36	-1.030500	-0.72188	-0.84625
15	F	8.3	1.665	13.45	-0.492940	-0.03167	-0.25903
16	M	7.6	1.827	12.84	-1.027100	-3.53450	-2.21390
17	M	8.1	2.029	15.35	2.015100	0.93011	1.74060
18	F	7.2	1.790	14.73	-1.164000	-1.11290	-1.19000

Table 1: GABA and NAA concentrations from midline occipital ROI as measured by MRS, and BOLD fMRI scores. Mean GABA level =1.823, SD = 0.135. Mean NAA level = 14.672, SD = 1.296 (n=18).